Front. Optoelectron. 2020, 13(4): 381–392
https://doi.org/10.1007/s12200-020-1096-x

RESEARCH ARTICLE

Line-field confocal optical coherence tomography for three-dimensional skin imaging

Jonas OGIEN[1], Anthony DAURES[1], Maxime CAZALAS[1], Jean-Luc PERROT[2], Arnaud DUBOIS (✉)[3]

1 DAMAE Medical, Paris 75013, France
2 CHU St-Etienne, Service Dermatologie, Saint-Etienne 42055, France
3 Université Paris-Saclay, Institut d'Optique Graduate School, CNRS, Laboratoire Charles Fabry, Palaiseau 91127, France

Abstract This paper reports on the latest advances in line-field confocal optical coherence tomography (LC-OCT), a recently invented imaging technology that now allows the generation of either horizontal ($x \times y$) section images at an adjustable depth or vertical ($x \times z$) section images at an adjustable lateral position, as well as three-dimensional images. For both two-dimensional imaging modes, images are acquired in real-time, with real-time control of the depth and lateral positions. Three-dimensional ($x \times y \times z$) images are acquired from a stack of horizontal section images. The device is in the form of a portable probe. The handle of the probe has a button and a scroll wheel allowing the user to control the imaging modes. Using a supercontinuum laser as a broadband light source and a high numerical microscope objective, an isotropic spatial resolution of ~1 μm is achieved. The field of view of the three-dimensional images is 1.2 mm × 0.5 mm × 0.5 mm ($x \times y \times z$). Images of skin tissues are presented to demonstrate the potential of the technology in dermatology.

Keywords optical coherence tomography (OCT), microscopy, three-dimensional imaging, dermatology

1 Introduction

Optical coherence tomography (OCT) is a technology based on low-coherence optical interferometry for imaging biological tissues with micrometer-scale spatial resolution [1,2]. OCT is commonly used in several medical fields [3], especially in ophthalmology to obtain images of the retina and the anterior segment of the eye [4]. OCT has begun to be used in interventional cardiology [5], and in gastroenterology for the detection and diagnosis of tumors [6,7]. OCT can be a useful tool for noninvasive imaging of brain tissues [8,9]. OCT also shows promise in dermatology to improve the diagnosis process of skin lesions [10].

In the field of dermatology, high spatial resolution imaging is necessary to resolve subtle morphological changes in skin tissues resulting from the early progression of lesions. Since the introduction of OCT about 30 years ago, significant progress has been achieved in the spatial resolution of OCT images. The axial resolution in OCT is governed by the temporal coherence of the illumination light source [2]. Improvement in the axial resolution of OCT images has been achieved through the emergence of efficient broadband light sources. Axial resolutions down to ~1 μm have been achieved with mode-locked lasers [11] and more recently with supercontinuum lasers [12–14]. The lateral resolution of the OCT images depends on how the light beam is focused on the sample [2]. Depending on whether the signal is acquired as a function of the optical frequency (in frequency/Fourier-domain OCT, referred to as FD-OCT) or as a function of time (in time-domain OCT, referred to as TD-OCT), the beam focusing constraints differ, which has an impact on the lateral resolution.

In TD-OCT, the reflectivity profile of the sample as a function of depth (an A-scan) is acquired by scanning the sample depth [1,2]. In FD-OCT, the reflectivity profile of the sample as a function of depth is acquired without scanning the depth, by measuring the spectrum of the interferometric signal [2]. In both TD-OCT and FD-OCT, a B-scan (a vertical section image) is then obtained by lateral scanning of the light beam to acquire several adjacent A-scans. En face images can also be obtained by scanning the beam in two lateral directions. En face imaging has been implemented in both TD-OCT and FD-OCT [15].

FD-OCT is superior to TD-OCT in terms of acquisition rate and detection sensitivity [16], but has shortcomings including a limited lateral resolution [17]. Since all points

Received September 5, 2020; accepted October 29, 2020

E-mail: arnaud.dubois@institutoptique.fr

in the depth range in the sample must be in focus simultaneously, a depth of field (DOF) at least equal to the depth range is needed, which limits the beam focusing. Several approaches have been reported to try to circumvent this limitation, i.e., improve the lateral resolution without sacrificing the imaging depth. One approach consists in increasing the DOF using Bessel beams produced by axicon lenses [17–20] or coaxially focused multimode beams [20] or apodized beams [21,22]. Computational methods have also been reported, such as interferometric synthetic aperture microscopy [23,24] or digital refocusing [25,26]. Another approach consists in overlapping and fusing several B-scans acquired at different depths by using a phase plate [27] or multiple light beams focused at different depths, in order to image over a depth range larger than the DOF [28,29]. This approach has also been combined with Bessel beam illumination [30], or using several beams with different wavelengths associated to different depths [31,32]. The B-scans to combine can also be obtained using a single beam refocused at different depths, a method referred to as C-mode scanning [33] or Gabor-domain OCT [34,35]. Let us note that this approach has also been combined with digital refocusing to improve its throughput [36].

Unlike FD-OCT, TD-OCT offers the possibility to continuously adjust the focus as a function of depth, making TD-OCT more suitable for producing images with high lateral resolution. Dynamic focus tracking in TD-OCT with free-space optics has been reported, but the tracking rate was slow [37,38]. A microelectromechanical systems (MEMS) mirror was designed for high-speed dynamic focus tracking, but without demonstration of the imaging capability *in vivo* [39]. Another approach consists of acquiring a sequence of images by gradually shifting the focus onto the sample and then fusing together the in-focus imaging zones [40]. This process results in a trade-off between lateral resolution and image acquisition speed. Another method is to collect multiple foci simultaneously with a multifocus fiber tip array [41]. Despite these advances, however, high lateral resolution TD-OCT imaging using dynamic focusing remains difficult since a high tracking speed is required.

Line-field confocal optical coherence tomography (LC-OCT) is a recently invented imaging technology that can produce images without the lateral resolution limitation of FD-OCT and without the speed limitation of conventional dynamically-focused TD-OCT. This paper reports on the latest LC-OCT prototype. Compared to the previous prototype capable of acquiring either horizontal (en face, $x \times y$) section images at an adjustable depth or vertical section images (B-scan, $x \times z$) at an adjustable lateral position [42], three-dimensional images ($x \times y \times z$) can also be acquired now. The technical characteristics of the different imaging modes are described. The device is now in the form of a portable probe. The handle of the probe has a button and a scroll wheel allowing the user to control the imaging modes. Three-dimensional images of skin tissues are presented to demonstrate the potential of LC-OCT in dermatology.

2 Line-field confocal optical coherence tomography technique

2.1 General principle and interest

LC-OCT is an imaging technique based on TD-OCT with illumination of the sample with a line of light and detection using a line camera [42–47]. This differs from conventional TD-OCT where the sample is illuminated point by point and a vertical section image is obtained from several A-scans acquired sequentially. In conventional TD-OCT, the scan of the sample depth is repeated after each A-scan acquisition, which requires depth scanning at high speed to obtain an image in real-time. In LC-OCT, all the A-scans of a vertical section image are acquired in parallel. The speed of the depth scan in LC-OCT can therefore be reduced compared to point-scanning TD-OCT, without increasing the image acquisition time. Producing a vertical section image in real-time with LC-OCT requires scanning the sample depth at a frequency of a few Hertz only. Obtaining a vertical section image at the same frame rate in point-scanning TD-OCT requires depth scanning at a frequency increased by a factor equal to the number of A-scans (factor of 2048 compared to LC-OCT using a line camera with 2048 pixels). The significantly slower depth scan in LC-OCT makes it possible to dynamically focus a microscope objective at a speed suitable for the real-time acquisition of high-resolution vertical section images. In LC-OCT, vertical section images can thus be obtained without the lateral resolution limitation of FD-OCT and without the speed limitation of conventional dynamically-focused TD-OCT. In addition, with the recent LC-OCT prototypes, it is also possible to obtain high-resolution horizontal section images by scanning the illumination line laterally on the sample [47].

2.2 Latest prototype

The experimental setup of the latest LC-OCT prototype is shown schematically in Fig. 1. It is based on a Linnik-type interferometer with a piezoelectric (PZT) stage for depth (z) scanning and a mirror galvanometer for lateral (y) scanning. The reference surface of the interferometer is mounted on a PZT chip that can oscillate to generate a phase modulation. A supercontinuum laser is used as a broadband light source at a detected central wavelength of about 750 nm. A cylindrical lens is employed to generate a line of light that is focused on the sample. The image of this line is projected on a line-scan camera. All the elements used for illumination and imaging (laser, optics, camera) are the same as those of the previously reported

LC-OCT system [47]. The microscope objectives are also the same (20×, numerical aperture (NA) of 0.5). Silicone oil is used as an immersion medium with a refractive index of 1.4, close to the mean refractive index of human skin. Glass plates are placed in both arms of the interferometer under the microscope objectives for subject stabilization and for providing a low reflectivity (3.5%) reference surface. The whole reference arm of the interferometer and the microscope objective in the sample arm (elements in the dashed frame in Fig. 1) are mounted on the PZT stage for vertical section imaging. The general operation of the device and the image display are controlled by a new C++ software. The device is now in the form of a portable probe (see Fig. 2). The dimensions of the probe are 215 mm (length) × 120 mm (width) × 208 mm (height) and the weight is 1.2 kg. A button on the probe handle allows the user to record an image in both real-time imaging modes (vertical or horizontal). A double-click on the button enables to switch from one real-time imaging mode to another. The probe handle is also equipped with a scroll wheel, which allows the user to adjust the lateral/depth positions in the horizontal/vertical real-time imaging modes. When clicked, the scroll wheel also allows the user to choose between video recording and three-dimensional acquisition.

3 Three imaging modes

Compared to the previous LC-OCT prototype capable of acquiring either horizontal (en face, $x \times y$) section images at an adjustable depth or vertical section images (B-scan, $x \times z$) at an adjustable lateral position [42], three-dimensional images ($x \times y \times z$) can now be acquired with the new device. The operating principle and the technical characteristics of the three imaging modes are described below.

3.1 Vertical section imaging

A vertical section image is acquired by activating the PZT stage to scan the sample depth. The displacement of the PZT stage is analogically controlled by a custom electronic board that sends a periodic driving current (see Fig. 3). The PZT oscillates at a frequency of $f_{PZT} = 8$ Hz according to asymmetrical sawthooths. The amplitude of the oscillation is 500 μm, but due to the nonlinearity of the PZT stage displacement at the edges of the sawtooths, the images are acquired over only 80% of the total amplitude of the oscillation. The vertical section images are thus acquired over an effective depth range of $Z = 400$ μm. The camera is synchronized with the oscillation of the PZT. The camera frame rate is set at 70 kHz, so that the step between two consecutive lines corresponds to a displacement of the PZT of $\delta = 71$ nm, i.e., to a phase shift of $\pi/2$. A stack of $Z/\delta = 5600$ lines is acquired during each positive slope of the depth scan. A vertical section image is obtained by processing the acquired stack using a five-frame fringe envelope detection algorithm [48]. Acquisition and processing of stacks is repeated continuously during the round-trips of the PZT stage. The images are displayed in real-time at 8 frames/s in logarithmic scale with auto-

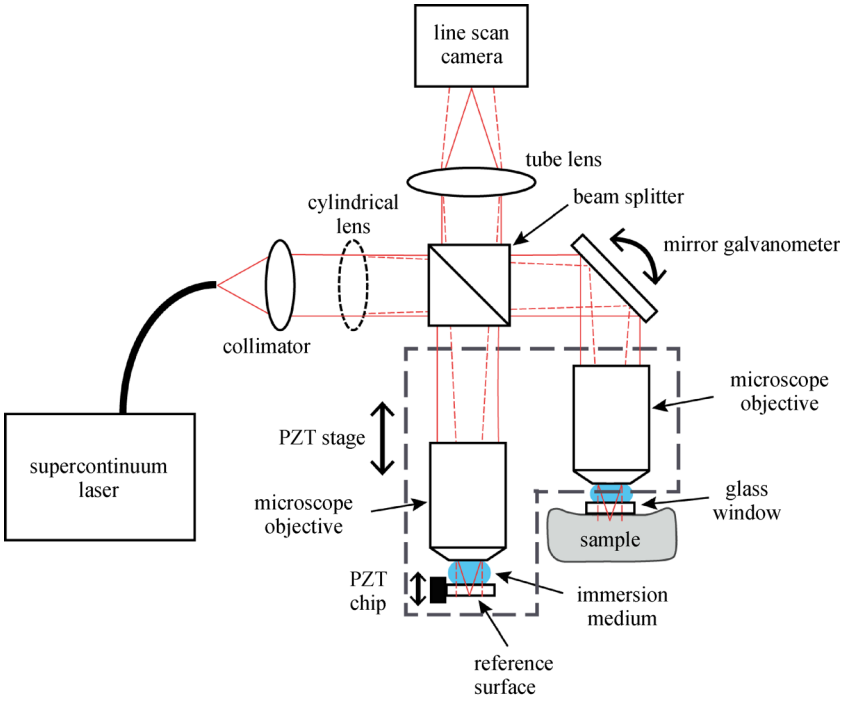

Fig. 1 Schematic diagram of the latest LC-OCT prototype

Fig. 2 LC-OCT probe and cart used by a dermatologist in a clinical setting

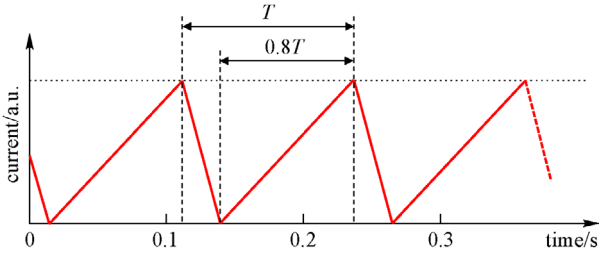

Fig. 3 Periodic current driving the oscillation of the PZT stage. The asymmetric triangle signal has a frequency of $f_{PZT} = 1/T = 8$ Hz and a duty cycle of 80%. Images are acquired only during the slow positive ramps

adjusted contrast after being appropriately rescaled. The size of each vertical section image is 2048 × 680 pixels ($x \times z$), corresponding to a field of view of 1.2 mm × 0.4 mm ($x \times z$).

In the vertical section imaging mode, the scroll wheel on the probe handle allows the user to modify the value of a direct current sent to the mirror galvanometer by the electronic board. This enables to laterally navigate within the sample being imaged, in real-time. The accuracy of the lateral position is determined by the noise in the rotation of the mirror galvanometer. In practice, the position of the laser line focused on the sample does not fluctuate more than the lateral resolution of the imaging system. Therefore, the positioning accuracy can be considered to be better than 1 μm. This is of course a much higher positioning resolution than can be achieved by moving the probe manually.

3.2 Horizontal section imaging

In the horizontal section imaging mode, the mirror galvanometer oscillates according to asymmetrical sawtooths, at a frequency $f_{galvo} = 8$ Hz (see Fig. 4), to scan the illumination line on the sample over a field of 500 μm. Let us note that the scanning field of 500 μm represents 95% of the total scanning amplitude of the mirror galvanometer, to avoid nonlinearities at the edges of the sawtooths. The mirror galvanometer is analogically controlled by the same custom electronic board as the PZT stage. The camera frame rate is set to $f_{cam} = 100$ Hz. Two consecutive lines acquired by the camera are thus separated by a lateral distance of 47 nm. A stack of 10600 lines is acquired during each positive slope of the lateral scan. The reference surface of the interferometer oscillates sinusoidally to generate a phase modulation. The current driving the oscillation is generated by the same custom electronic

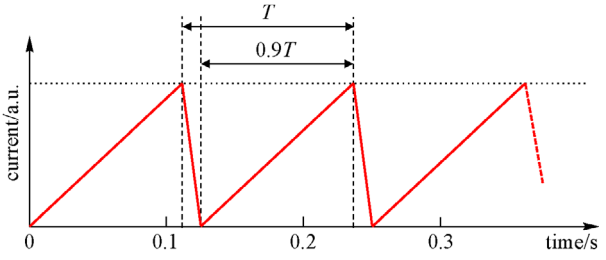

Fig. 4 Periodic current driving the oscillation of the mirror galvanometer. The asymmetric triangle signal has a frequency of $f_{galvo} = 1/T = 8$ Hz and a duty cycle of 90%. Images are acquired only during the slow positive ramps

board that controls the PZT stage and the mirror galvanometer. It is amplified before being sent to the PZT chip. A sinusoidal phase-shifting algorithm is used to calculate each line of the horizontal section image from an algebraic combination of five consecutive lines acquired by the camera [48]. The frequency of the phase modulation and its amplitude are set empirically at 8 kHz and 1 μm respectively to optimize the image quality. Acquisition and processing is repeated continuously during the round-trips of the mirror galvanometer. The horizontal section images are displayed in real-time at 8 frames/s in logarithmic scale with auto-adjusted contrast after being appropriately rescaled. The size of each horizontal section image is 2048 × 850 pixels ($x \times y$), corresponding to a field of view of 1.2 mm × 0.5 mm ($x \times y$).

In the horizontal section imaging mode, the scroll wheel on the probe handle allows the user to control the value of a direct current sent to the PZT stage by the electronic board. This makes it possible to control at what depth the sample is imaged, between 0 and 500 μm, in real-time and with an accuracy determined by the resolution of the PZT stage which is much better than the axial resolution of the imaging system of ~1 μm.

3.3 Three-dimensional imaging

Three-dimensional images can be produced from a stack of horizontal section images acquired at successive depths. In the three-dimensional imaging mode, horizontal section images are continuously acquired while a ramp signal is sent by the electronic board to the PZT stage to displace it from 0 to 500 μm. The ramp signal is adjusted so that successive horizontal section images correspond to a depth difference of one micrometer, approximately equal to the axial resolution of the imaging system. This results in three-dimensional stacks of 2048 × 850 × 500 pixels, scaled to 1200 × 500 × 500 pixels for proper aspect ratio. The three-dimensional images correspond to a volume of up to 1.2 mm × 0.5 mm × 0.5 mm ($x \times y \times z$).

Since the PZT stage moves continuously during the lateral scan with the mirror galvanometer, the images of a stack are not perfectly horizontal. However, since the depth difference between the edges of each image of a stack is one micrometer, the tilt is imperceptible. Let us note that the implementation of this acquisition scheme (continuous imaging over a continuous ramp) is simple, as it requires no particular synchronization between the PZT stage and the mirror galvanometer.

In practice, three-dimensional imaging is decided by the user by clicking the scroll wheel of the probe handle and turning it to the appropriate direction. One direction of rotation initiates the acquisition of a three-dimensional image, while the other direction initiates a video recording of the current imaging mode. The effect of rotating the scroll wheel back and forward is shown on the software display window when the user clicks on the scroll wheel. Once a three-dimensional acquisition has started, the PZT stage and the mirror galvanometer move continuously until the PZT stage reaches its maximum depth of 500 μm. When the maximum depth is reached, the horizontal image acquisition stops and the system returns to the imaging mode it was in before the three-dimensional acquisition was performed. In the three-dimensional imaging mode, the acquired horizontal images are displayed and the user can stop the acquisition whenever he wants, without waiting for the PZT stage to reach its maximum depth, by clicking on the scroll wheel or on the button on the probe handle. In that case, the depth of the acquired volumetric image is less than 500 μm and depends on when the user stopped the acquisition.

4 Skin imaging

LC-OCT has previously been shown to yield high quality imaging of human skin, *in vivo*, giving access non-invasively to a level of morphological detail close to the one of histology using similar microscope objectives (20×, NA = 0.5) [43,49–60]. The latest LC-OCT prototype introduced here was also designed specifically for *in vivo* skin imaging. The skin is gently pressed again the glass window in the sample arm of the interferometer in order to hold it steady, flatten it, and maintain it at the position corresponding to the working distance of the microscope objective. A drop of paraffin oil is placed between the skin and the glass window in order to minimize parasitic reflections at the interfaces.

Figure 5 illustrates the performance of the LC-OCT prototype for the two real-time imaging modes. The images were obtained from healthy skin of a 30-year-old man. Three horizontal section images are shown for three different depths corresponding to different layers of the skin (*stratum spinosum*, *stratum basale*, superficial dermis). In the *stratum spinosum* (Fig. 5(a)), the dark spots correspond to the nuclei of keratinocyte cells. Melanin, which appears as bright spots, is well resolved in the *stratum basale* (Fig. 5(b)), along with keratinocyte cells presenting a higher density than in the *stratum spinosum*, with a smaller size. The network of fibers formed by collagen and elastin within the dermis is also visible (Fig. 5(c)), with the possibility to identify single fibers in some regions. A vertical section image is also shown (Fig. 5(d)), where the different layers of the skin can be identified, in particular the epidermis (including the *stratum corneum*) and the dermis, and the dermal-epidermal junction which separates them (which appears dark). Nuclei of keratinocyte cells are well resolved as they were in the horizontal mode. Within the dermis, blood vessels, which appear dark, can be identified.

The main novelty of the prototype is to be able to acquire

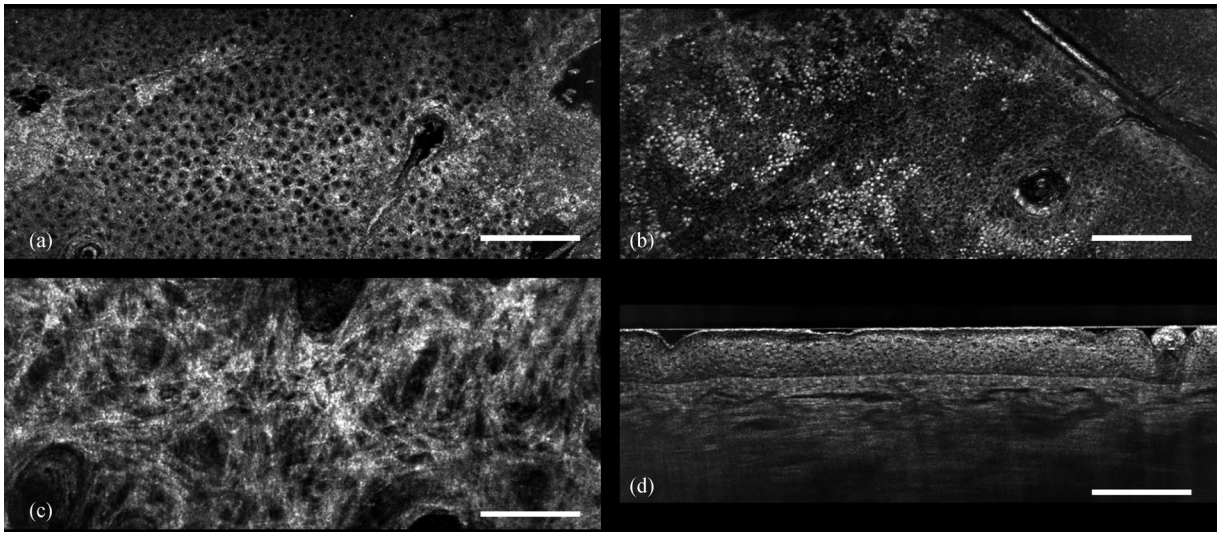

Fig. 5 LC-OCT images of healthy human skin *in vivo* obtained in real-time (8 frames/s). Horizontal section images obtained at the level of the *stratum spinosum* (a), the *stratum basale* (b) and the superficial dermis (c). A vertical section image is also displayed (d). Scale bars are 200 μm

three-dimensional images of skin, *in vivo*, once a region of interest has been identified by examining it using the real-time horizontal and vertical imaging modes. Owing to the quasi-isotropic resolution of LC-OCT close to 1 μm, the volume rendering images exhibit morphological information at cellular level in three-dimensions, and can be regarded as "histological blocks", revealing morphological features inaccessible in conventional histology where only slices in two dimensions can be analyzed.

Figure 6 shows several views of a LC-OCT volume rendering image of *in vivo* healthy skin, acquired on the skin of a 30-year-old man. Three-dimensional visualization was obtained using the volume rendering module of the open-source software 3D Slicer. The features that were visible in the horizontal and vertical images can now be visualized in three dimensions, including for instance the skin layers and the dermal-epidermal junction, the nuclei of keratinocyte cells, elastin and collagen fibers, and blood vessels.

Three-dimensional imaging offers several valuable ways to visualize the data for analysis. It is possible to reslice the volume along any plane of interest. In particular, it is possible to obtain vertical and horizontal images from the volume, similar to the images obtained during real-time acquisition, as shown in Fig. 7(a). It is also possible to navigate within the volume while visualizing such vertical and horizontal images, as shown in Fig. 7(b).

Other types of visualizations can be useful to analyze given features in three-dimension within the skin. Figure 8 shows for example a three-dimensional maximum intensity projection applied to a sub-region of a volume obtained *in vivo* on the palm of the hand, a site where the *stratum corneum* is very thick, yielding helicoidal sweat ducts. This technique consists in displaying the brightest voxel value encountered in each projection line of the rendered volume. As the sweat ducts are hyperreflective, the maximum intensity projection enables to clearly visualize them in three-dimensions.

Conversely, a minimum intensity projection exhibits the three-dimensional aspect of hyporeflective structures, by displaying the darkest voxel value encountered in each projection line of the rendered volume. In particular, blood vessels can be visualized using this type of projection. Figure 9 shows for example a three-dimensional minimum intensity projection applied to a sub-region of a volume obtained *in vivo* at the level of the nailfold. Several well organized long looped capillaries can be observed. The analysis (capillaroscopy) of the capillaries in the region of the nailfold can be useful for the diagnosis of several diseases [61]. The application of a minimum intensity projection to the LC-OCT volumetric images enables to visualize those capillaries in three-dimensions, which is not feasible using conventional capillaroscopy methods.

Eventually, let us note that three-dimensional cellular level imaging opens the way for more relevant quantification metrics of the skin, as the metrics can be obtained from full volumes. This includes for instance the keratinocyte cells or melanin distribution and density within the epidermis, or the quantification of the dermal-epidermal junction and of the epidermis thickness, which can be obtained from the segmentation of the epidermis and dermis from a three-dimensional image, as shown in Fig. 10. The three-dimensional visualization of the segmentation was obtained using the segmentation module of 3D Slicer, applied to a volume previously segmented by hand using the open-source software ImageJ.

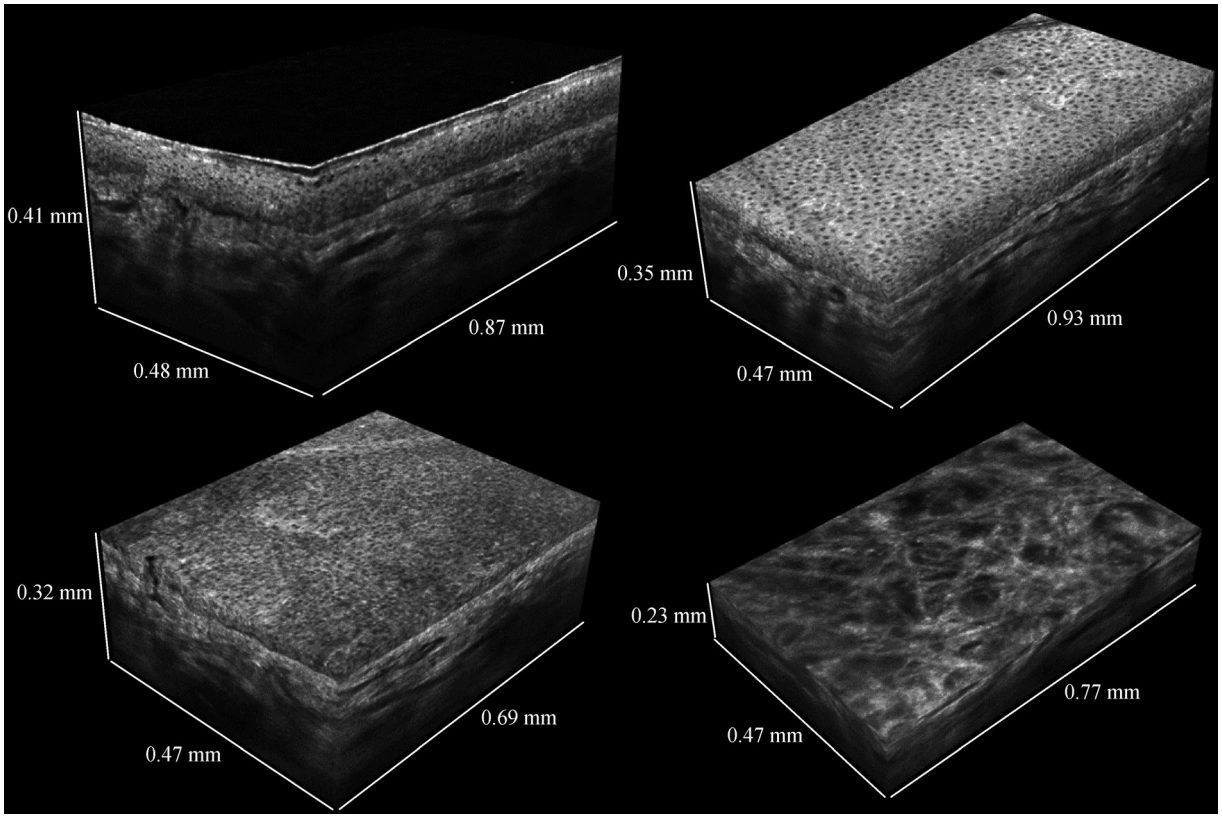

Fig. 6 Three-dimensional volume rendering of *in vivo* human healthy skin, digitally "cut" at different depths

5 Conclusions

A new LC-OCT prototype has been developed to generate both vertical section images and horizontal section images, as well as three-dimensional images. The device is in the form of a portable probe. The handle of the probe has a button and a scroll wheel for an easy control of the imaging modes. The vertical section images have a field of view of 1.2 mm × 0.4 mm ($x \times z$) and the horizontal section images have a field of view of 1.2 mm × 0.5 mm ($x \times y$). The images have a quasi-isotropic spatial resolution of ~1 μm. They are acquired and displayed at a frame rate of 8 Hz in both modes. The three-dimensional images are acquired from a stack of horizontal section images acquired down to a depth of 0.5 mm. They correspond to a volume of up to 1.2 mm × 0.5 mm × 0.5 mm ($x \times y \times z$).

In vivo imaging of human skin at the cellular level was demonstrated in both vertical and horizontal imaging modes. Three-dimensional cellular level imaging of human skin, *in vivo*, was also demonstrated. The acquisition of three-dimensional data sets enables subsequent analysis of a volume of the skin at cellular resolution, assimilable to a "histological block", and revealing morphological features inaccessible in conventional histology where only two-dimensional slices can be analyzed. Three-dimensional imaging also allows for different types of visualization and segmentation, which can be useful for better understanding the morphology of certain structures, revealing their sizes, shapes, three-dimensional distribution, and connections with other structures. The information provided by three-dimensional analysis could also be relevant for establishing new, more relevant quantification metrics of the skin.

The effective imaging depth in skin tissues with the LC-OCT prototype reported here is limited by light scattering to ~400 μm. Deeper penetration can be achieved with FD-OCT devices operating at longer wavelengths (around 1300 nm). These devices benefit from both higher detection sensitivity and less light scattering in tissues, but do not offer a spatial resolution as high as LC-OCT.

From a technological point of view, progress could still be made in terms of compactness and weight of the hand-held probe. An approach currently being considered would be to develop an LC-OCT device with three-dimensional imaging capabilities based on a Mirau interferometer rather than a Linnik interferometer [46,62]. The frame rate of the vertical section imaging mode is currently limited at 8 Hz by the mechanical response of the PZT stage to a triangle driving signal and not by camera speed or the power of the light source. The frame rate could be increased by driving the PZT stage with a sinusoidal signal and operating the camera at a variable frequency. Such a hand-held LC-OCT probe with reduced weight and higher image acquisition speed would facilitate the use of the technology by dermatologists in daily practice.

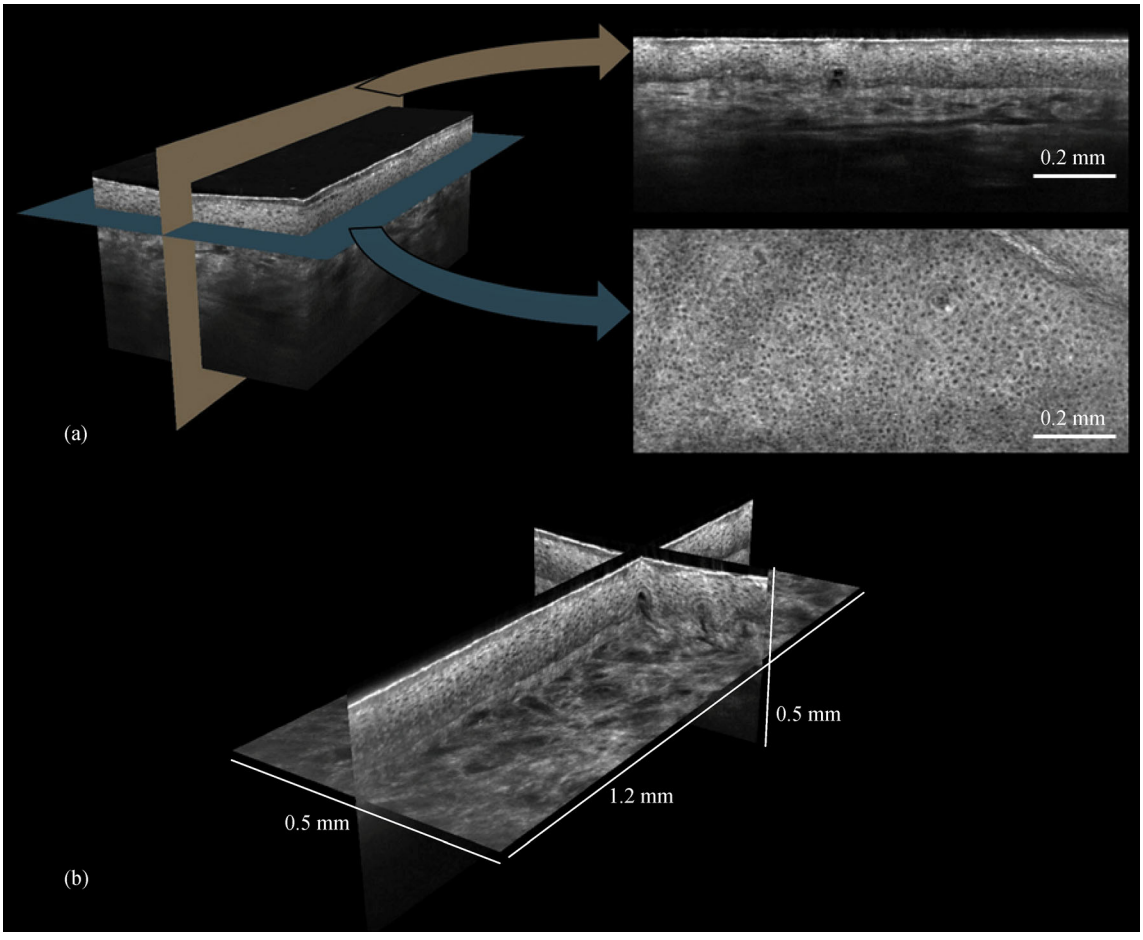

Fig. 7 (a) Vertical and horizontal cross-section images obtained from a three-dimensional LC-OCT image. (b) Three-dimensional visualization from vertical and horizontal cross-section images

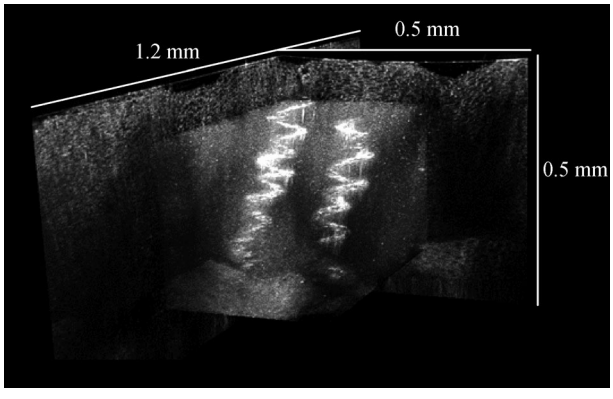

Fig. 8 Three-dimensional visualization of sweat ducts of the palm of the hand from application of a maximum intensity projection to a three-dimensional LC-OCT image

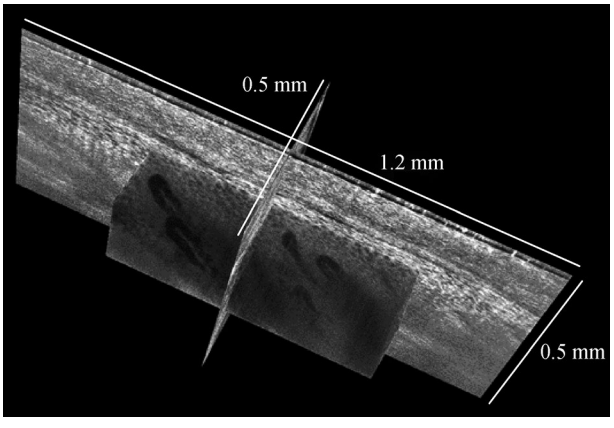

Fig. 9 Three-dimensional visualization of capillaries of the nailfold from application of a minimum intensity projection to a three-dimensional LC-OCT image

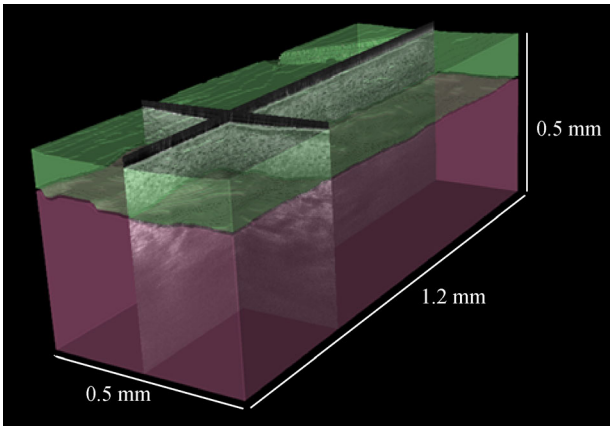

Fig. 10 Skin layers segmentation of a three-dimensional LC-OCT image. The green volume corresponds to the segmented epidermis, while the purple volume corresponds to the dermis

In terms of applications of the technology, clinical studies are currently being conducted with the new LC-OCT imaging device to demonstrate the potential in dermatology for the non-invasive diagnosis of early-stage skin cancers.

Acknowledgements The authors thank the whole team of engineers at DAMAE Medical, especially Olivier Levecq, Hicham Azimani, Emmanuel Cohen and Romain Allemand, for their work on the technology and design of the LC-OCT prototype presented in this paper. They also thank Amyn Kassara for providing the segmentation of the three-dimensional images. They are also grateful to Anaïs Barut and David Siret as directors and managers of DAMAE Medical.

References

1. Fercher A F. Optical coherence tomography. Journal of Biomedical Optics, 1996, 1(2): 157–173
2. Podoleanu A G. Optical coherence tomography. Journal of Microscopy, 2012, 247(3): 209–219
3. Zysk A M, Nguyen F T, Oldenburg A L, Marks D L, Boppart S A. Optical coherence tomography: a review of clinical development from bench to bedside. Journal of Biomedical Optics, 2007, 12(5): 051403
4. Schuman J S, Puliafito C A, Fujimoto J G, Duker J S. Optical Coherence Tomography of Ocular Diseases. 3rd ed. New Jersey: Slack Inc., 2013
5. Bezerra H G, Costa M A, Guagliumi G, Rollins A M, Simon D I. Intracoronary optical coherence tomography: a comprehensive review clinical and research applications. JACC: Cardiovascular Interventions, 2009, 2(11): 1035–1046
6. Adler D C, Chen Y, Huber R, Schmitt J, Connolly J, Fujimoto J G. Three-dimensional endomicroscopy using optical coherence tomography. Nature Photonics, 2007, 1(12): 709–716
7. Yu X, Ding Q, Hu C, Mu G, Deng Y, Luo Y, Yuan Z, Yu H, Liu L. Evaluating micro-optical coherence tomography as a feasible imaging tool for pancreatic disease diagnosis. IEEE Journal of Selected Topics in Quantum Electronics, 2019, 25(1): 1–8
8. Men J, Huang Y, Solanki J, Zeng X, Alex A, Jerwick J, Zhang Z, Tanzi R E, Li A, Zhou C. Optical coherence tomography for brain imaging and developmental biology. IEEE Journal of Selected Topics in Quantum Electronics, 2016, 22(4): 120–132
9. Fan Y, Xia Y, Zhang X, Sun Y, Tang J, Zhang L, Liao H. Optical coherence tomography for precision brain imaging, neurosurgical guidance and minimally invasive theranostics. Bioscience Trends, 2018, 12(1): 12–23
10. Levine A, Wang K, Markowitz O. Optical coherence tomography in the diagnosis of skin cancer. Dermatologic Clinics, 2017, 35(4): 465–488
11. Drexler W, Morgner U, Kärtner F X, Pitris C, Boppart S A, Li X D, Ippen E P, Fujimoto J G. *In vivo* ultrahigh-resolution optical coherence tomography. Optics Letters, 1999, 24(17): 1221–1223
12. Povazay B, Bizheva K, Unterhuber A, Hermann B, Sattmann H, Fercher A F, Drexler W, Apolonski A, Wadsworth W J, Knight J C, Russell P S J, Vetterlein M, Scherzer E. Submicrometer axial resolution optical coherence tomography. Optics Letters, 2002, 27 (20): 1800–1802
13. Wang Y, Zhao Y, Nelson J S, Chen Z, Windeler R S. Ultrahigh-resolution optical coherence tomography by broadband continuum generation from a photonic crystal fiber. Optics Letters, 2003, 28(3): 182–184
14. Aguirre A, Nishizawa N, Fujimoto J, Seitz W, Lederer M, Kopf D. Continuum generation in a novel photonic crystal fiber for ultrahigh resolution optical coherence tomography at 800 nm and 1300 nm. Optics Express, 2006, 14(3): 1145–1160
15. Leitgeb R A. En face optical coherence tomography: a technology review. Biomedical Optics Express, 2019, 10(5): 2177–2201
16. Choma M, Sarunic M, Yang C, Izatt J. Sensitivity advantage of swept source and Fourier domain optical coherence tomography. Optics Express, 2003, 11(18): 2183–2189
17. Lee K S, Rolland J P. Bessel beam spectral-domain high-resolution optical coherence tomography with micro-optic axicon providing extended focusing range. Optics Letters, 2008, 33(15): 1696–1698
18. Leitgeb R A, Villiger M, Bachmann A H, Steinmann L, Lasser T. Extended focus depth for Fourier domain optical coherence microscopy. Optics Letters, 2006, 31(16): 2450–2452
19. Tamborski S, Lyu H C, Dolezyczek H, Malinowska M, Wilczynski G, Szlag D, Lasser T, Wojtkowski M, Szkulmowski M. Extended-focus optical coherence microscopy for high-resolution imaging of the murine brain. Biomedical Optics Express, 2016, 7(11): 4400–4414
20. Liu L, Chu K K, Houser G H, Diephuis B J, Li Y, Wilsterman E J, Shastry S, Dierksen G, Birket S E, Mazur M, Byan-Parker S, Grizzle W E, Sorscher E J, Rowe S M, Tearney G J. Method for quantitative study of airway functional microanatomy using micro-optical coherence tomography. PLoS One, 2013, 8(1): e54473
21. Liu L, Liu C, Howe W C, Sheppard C J R, Chen N. Binary-phase spatial filter for real-time swept-source optical coherence microscopy. Optics Letters, 2007, 32(16): 2375–2377

22. Yin B, Chu K K, Liang C P, Singh K, Reddy R, Tearney G J. μOCT imaging using depth of focus extension by self-imaging wavefront division in a common-path fiber optic probe. Optics Express, 2016, 24(5): 5555–5564
23. Ralston T S, Marks D L, Carney P S, Boppart S A. Interferometric synthetic aperture microscopy. Nature Physics, 2007, 3(2): 129–134
24. Coquoz S, Bouwens A, Marchand P J, Extermann J, Lasser T. Interferometric synthetic aperture microscopy for extended focus optical coherence microscopy. Optics Express, 2017, 25(24): 30807–30819
25. Yu L, Rao B, Zhang J, Su J, Wang Q, Guo S, Chen Z. Improved lateral resolution in optical coherence tomography by digital focusing using two-dimensional numerical diffraction method. Optics Express, 2007, 15(12): 7634–7641
26. Fechtig D J, Kumar A, Drexler W, Leitgeb R A. Full range line-field parallel swept source imaging utilizing digital refocusing. Journal of Modern Optics, 2015, 62(21): 1801–1807
27. Mo J, de Groot M, de Boer J F. Focus-extension by depth-encoded synthetic aperture in optical coherence tomography. Optics Express, 2013, 21(8): 10048–10061
28. Holmes J. Theory and applications of multi-beam OCT. In: Proceedings of the 1st Canterbury Workshop on Optical Coherence Tomography and Adaptive Optics. Canterbury: SPIE, 2008
29. Holmes J, Hattersley S, Stone N, Bazant-Hegemark F, Barr H. Multi-channel fourier domain OCT system with superior lateral resolution for biomedical applications. In: Proceedings of Coherence Domain Optical Methods and Optical Coherence Tomography in Biomedicine XII. San Jose: SPIE, 2008
30. Yi L, Sun L, Ding W. Multifocal spectral-domain optical coherence tomography based on Bessel beam for extended imaging depth. Journal of Biomedical Optics, 2017, 22(10): 1–8
31. Li J, Luo Y, Wang X, Wang N, Bo E, Chen S, Chen S, Chen S, Tsai M T, Liu L. Extending the depth of focus of fiber-optic optical coherence tomography using a chromatic dual-focus design. Applied Optics, 2018, 57(21): 6040–6046
32. Nam A S, Ren J, Bouma B E, Vakoc B J. Demonstration of triband multi-focal imaging with optical coherence tomography. Applied Sciences (Basel, Switzerland), 2018, 8(12): 2395
33. Huber R, Wojtkowski M, Fujimoto J G, Jiang J Y, Cable A E. Three-dimensional and C-mode OCT imaging with a compact, frequency swept laser source at 1300 nm. Optics Express, 2005, 13(26): 10523–10538
34. Rolland J P, Meemon P, Murali S, Thompson K P, Lee K S. Gabor-based fusion technique for optical coherence microscopy. Optics Express, 2010, 18(4): 3632–3642
35. Lee K S, Thompson K P, Meemon P, Rolland J P. Cellular resolution optical coherence microscopy with high acquisition speed for *in-vivo* human skin volumetric imaging. Optics Letters, 2011, 36 (12): 2221–2223
36. Liu S, Mulligan J A, Adie S G. Volumetric optical coherence microscopy with a high space-bandwidth-time product enabled by hybrid adaptive optics. Biomedical Optics Express, 2018, 9(7): 3137–3152
37. Schmitt J M, Lee S L, Yung K M. An optical coherence microscope with enhanced resolving power in thick tissue. Optics Communications, 1997, 142(4–6): 203–207
38. Lexer F, Hitzenberger C K, Drexler W, Molebny S, Sattmann H, Sticker M, Fercher A F. Dynamic coherent focus OCT with depth-independent transversal resolution. Journal of Modern Optics, 1999, 46(3): 541–553
39. Qi P A, Himmer P A, Gordon M L, Yang V X D, Dickensheets D L, Vitkin I A. Dynamic focus control in high-speed optical coherence tomography based on a microelectromechanical mirror. Optics Communications, 2004, 232(1–6): 123–128
40. Divetia A, Hsieh T H, Zhang J, Chen Z, Bachman M, Li G P. Dynamically focused optical coherence tomography for endoscopic applications. Applied Physics Letters, 2005, 86(10): 103902
41. Yang V X D, Munce N, Pekar J, Gordon M L, Lo S, Marcon N E, Wilson B C, Vitkin I A. Micromachined array tip for multifocus fiber-based optical coherence tomography. Optics Letters, 2004, 29 (15): 1754–1756
42. Dubois A, Levecq O, Azimani H, Davis A, Ogien J, Siret D, Barut A. Line-field confocal time-domain optical coherence tomography with dynamic focusing. Optics Express, 2018, 26(26): 33534–33542
43. Dubois A, Levecq O, Azimani H, Siret D, Barut A, Suppa M, Del Marmol V, Malvehy J, Cinotti E, Rubegni P, Perrot J L. Line-field confocal optical coherence tomography for high-resolution non-invasive imaging of skin tumors. Journal of Biomedical Optics, 2018, 23(10): 1–9
44. Ogien J, Siret D, Levecq O, Azimani H, David A, Xue W, Perrot J L, Dubois A. Line-field confocal optical coherence tomography. In: Proceedings of Optical Coherence Tomography and Coherence Domain Optical Methods in Biomedicine XXIII. San Francisco: SPIE, 2019
45. Davis A, Levecq O, Azimani H, Siret D, Dubois A. Simultaneous dual-band line-field confocal optical coherence tomography: application to skin imaging. Biomedical Optics Express, 2019, 10 (2): 694–706
46. Dubois A, Xue W, Levecq O, Bulkin P, Coutrot A L, Ogien J. Mirau-based line-field confocal optical coherence tomography. Optics Express, 2020, 28(6): 7918–7927
47. Ogien J, Levecq O, Azimani H, Dubois A. Dual-mode line-field confocal optical coherence tomography for ultrahigh-resolution vertical and horizontal section imaging of human skin *in vivo*. Biomedical Optics Express, 2020, 11(3): 1327–1335
48. Larkin K G. Efficient nonlinear algorithm for envelope detection in white light interferometry. Journal of the Optical Society of America A, Optics, Image Science, and Vision, 1996, 13(4): 832–843
49. Cazalas M, Levecq O, Azimani H, Siret D, Barut A, Suppa M, del Marmol V, Malvehy J, Cinotti E, Rubegni P, Perrot J L, Dubois A. Skin lesion imaging with line-field confocal optical coherence tomography. In: Proceedings of Photonics in Dermatology and Plastic Surgery 2019. San Francisco: SPIE, 2019
50. Dejonckheere G, Suppa M, Marmol V, Meyer T, Stockfleth E. The actinic dysplasia syndrome-diagnostic approaches defining a new

concept in field carcinogenesis with multiple cSCC. Journal of the European Academy of Dermatology and Venereology, 2019, 33 (S8): 16–20
51. Pedrazzani M, Breugnot J, Rouaud-Tinguely P, Cazalas M, Davis A, Bordes S, Dubois A, Closs B. Comparison of line-field confocal optical coherence tomography images with histological sections: validation of a new method for *in vivo* and non-invasive quantification of superficial dermis thickness. Skin Research and Technology, 2020, 26(3): 398–404
52. Ogien J, Levecq O, Cazalas M, Suppa M, del Marmol V, Malvehy J, Cinotti E, Rubegni P, Perrot J L, Dubois A. Handheld line-field confocal optical coherence tomography for dermatology. In: Proceedings of Photonics in Dermatology and Plastic Surgery 2020. San Francisco: SPIE, 2020
53. Monnier J, Tognetti L, Miyamoto M, Suppa M, Cinotti E, Fontaine M, Perez J, Orte Cano C, Yélamos O, Puig S, Dubois A, Rubegni P, Marmol V, Malvehy J, Perrot J L. *In vivo* characterization of healthy human skin with a novel, non-invasive imaging technique: line-field confocal optical coherence tomography. Journal of the European Academy of Dermatology and Venereology, 2020, doi:10.1111/jdv.16857
54. Ruini C, Sattler E. Line-field confocal optical coherence tomography: the golden goose? Aktuelle Dermatologie, 2020, 46: 148–151
55. Tognetti L, Rizzo A, Fiorani D, Cinotti E, Perrot J L, Rubegni P. New findings in non-invasive imaging of aquagenic keratoderma: Line-field optical coherence tomography, dermoscopy and reflectance confocal microscopy. Skin Research and Technology, 2020, doi:10.1111/srt.12882
56. Ruini C, Schuh S, Sattler E, Welzel J. Line-field confocal optical coherence tomography–practical applications in dermatology and comparison with established imaging methods. Skin Research and Technology, 2020, doi:10.1111/srt.12949
57. Tognetti L, Fiorani D, Cinotti E, Rubegni P. Tridimensional skin imaging in aquagenic keratoderma: virtual histology by line-field confocal optical coherence tomography. International Journal of Dermatology, 2020, doi:10.1111/ijd.15169
58. Tognetti L, Fiorani D, Suppa M, Cinotti E, Fontaine M, Marmol V D, Rubegni P, Perrot J L. Examination of circumscribed palmar hypokeratosis with line-field confocal optical coherence tomography: dermoscopic, ultrasonographic and histopathologic correlates. Indian Journal of Dermatology, Venereology and Leprology, 2020, 86(2): 206–208
59. Tognetti L, Carraro A, Lamberti A, Cinotti E, Suppa M, Luc Perrot J, Rubegni P. Kaposi sarcoma of the glans: new findings by line field confocal optical coherence tomography examination. Skin Research and Technology, 2020, doi:10.1111/srt.12938
60. Ruini C, Schuh S, Pellacani G, French L, Welzel J, Sattler E. *In vivo* imaging of Sarcoptes scabiei infestation using line-field confocal optical coherence tomography. Journal of the European Academy of Dermatology and Venereology, 2020, doi:10.1111/jdv.16671
61. Rennie D. Nailfold dermatoscopy in general practice. Australian Family Physician, 2015, 44(11): 809–812
62. Xue W, Ogien J, Levecq O, Dubois A. Line-field confocal optical coherence tomography based on a Mirau interferometer. In: Proceedings of Unconventional Optical Imaging II. SPIE, 2020

Jonas Ogien received his M.S. degree in Optics in 2014 from University of Rochester (USA) and his Ph.D. degree in Physics in 2017 from Paris-Saclay University (France). He also holds an engineering degree from Institut d'Optique Graduate School (France) and currently works as a research engineer at DAMAE Medical, a startup company working on OCT for skin imaging. He is particularly interested in innovative optical methods for high-resolution imaging. His current research focuses on the development of new modalities and optical improvements in OCT.

Anthony Daures received his engineering degree in Physics from Institut National des Sciences Appliquées in Toulouse (France) in 2014. He also holds an M.S. degree in Medical Imaging from University of Paul Sabatier (Toulouse, France). As an image processing engineer with more than seven years of experience, he has worked for different medical imaging companies and has always focused on the development of innovative algorithms. He is currently working as an image quality engineer at DAMAE Medical to improve diagnosis in real-time.

Maxime Cazalas, M.Sc., is a computer science and image processing engineer with over 14 years of experience in medical imaging. Passionate about innovation in the field of medical imaging, he has been involved in the development of new and innovative imaging solutions to assist physicians in delivering the best possible care to their patient. Maxime is currently focused on dermato-oncology, using *in vivo* optical imaging technics to better understand the pathogenesis of skin tumors, enabling earlier diagnosis and optimal patient-tailored therapy.

Jean-Luc Perrot, Ph.D. & M.D., has a 30-year career as a dermatologist and medical oncologist at Saint-Etienne University Hospital (France). He was the former president of the non-invasive skin imaging group of the French Society of Dermatology. Multimodal skin imaging has developed considerably in his dermatology department where different optical techniques are combined, including confocal microscopy, OCT, LC-OCT, dermatoscopy and Raman spectroscopy. Perrot has been involved in the validation and/or design of several innovative imaging devices. Although he has published numerous books on skin imaging, his primary objective remains the management of patients in the context of daily practice.

Arnaud Dubois received his Ph.D. degree in Physics in 1997 from Paris-Saclay University (France). Since 2006, he is a professor of optics at Université Paris-Saclay, Institut d'Optique Graduate School (France). Pioneer in full-field OCT in the early 2000, Dubois has since been a major contributor to the development of this technology. He has published 120 research articles in scientific journals and conference proceedings and 12 book chapters. He was the scientific editor in 2016 of the first and only handbook entirely devoted to full-field OCT. In 2014, Dubois co-founded DAMAE Medical, a startup company working on an innovative OCT technique for skin imaging.